Journal Pre-proof

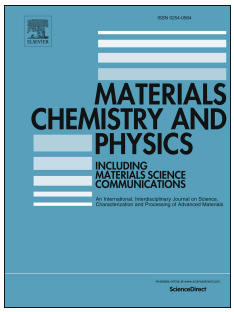

Nanocomposite Co-nSiC coatings electrodeposited from cobalt-gluconate bath via pulse reverse plating technique with anionic surfactant

D.P. Weston, D. Albusalih, H. Hilton-Tapp, D. Statharas, S.P. Gill, J. Navajas, J. Cornec, N.J. Weston

PII: S0254-0584(23)00651-X

DOI: https://doi.org/10.1016/j.matchemphys.2023.127943

Reference: MAC 127943

To appear in: *Materials Chemistry and Physics*

Received Date: 10 January 2023

Revised Date: 9 March 2023

Accepted Date: 18 May 2023

Please cite this article as: D.P. Weston, D. Albusalih, H. Hilton-Tapp, D. Statharas, S.P. Gill, J. Navajas, J. Cornec, N.J. Weston, Nanocomposite Co-nSiC coatings electrodeposited from cobalt-gluconate bath via pulse reverse plating technique with anionic surfactant, *Materials Chemistry and Physics* (2023), doi: https://doi.org/10.1016/j.matchemphys.2023.127943.

D. P. Weston	Conceptualisation, Methodology, Investigation, Visualisation, Writing - Original Draft, Supervision, Writing - Review & Editing
D Albusalih	Methodology, Investigation, Writing - Review & Editing, Data Curation
H Hilton-Tapp	Writing - Review & Editing, Data Curation
D Statharas,	Writing - Review & Editing, Data Curation
S. P. Gill,	Data Curation, Methodology
J Navajas	Investigation
J Cornec,	Investigation
N.J. Weston	Conceptualisation, Methodology

Nanocomposite Co-nSiC Coatings Electrodeposited from Cobalt-Gluconate Bath via Pulse Reverse Plating Technique with Anionic Surfactant

D. P. Weston*, D Albusalih, H Hilton-Tapp, D Statharas, S. P. Gill, J Navajas, J Cornec, N.J. Weston[1].

COVER SHEET

Nanocomposite Co-nSiC Coatings Electrodeposited from Cobalt-Gluconate Bath via Pulse Reverse Plating Technique with Anionic Surfactant

D. P. Weston*, D Albusalih, H Hilton-Tapp, D Statharas, S. P. Gill, J Navajas, J Cornec, N.J. Weston[1].

Mechanics of Materials Group, Department of Engineering, University of Leicester, LE7 1RH, UK

[1] Department of Mechanics, Materials and Structures, Faculty of Engineering, University of Nottingham, University Park, Nottingham NG7 2RD, UK.

** corresponding author: dpw14@le.ac.uk*

Abstract.

The co-deposition of silicon carbide nanoparticles (50±5 nm diameter) in an electrodeposited metallic cobalt matrix has been investigated under pulse reverse plating (PRP) conditions with the inclusion of an anionic surfactant. The effect of variable anionic surfactant content in the plating solution with a particle content of 5 g L^{-1} was evaluated using both direct current (DC) plating and PRP. The particle content of the coatings was investigated by varying the cathodic cycle during PRP by varying the cathodic cycle time between 30 to 240 seconds per pulse whilst maintaining a fixed anodic charge. The coatings were assessed by SEM and EDX in cross section to determine the effect of PRP parameters and anionic surfactant content on the particle content of. With no anionic surfactant, all coatings produced contained a similar particle content. Addition of anionic surfactant affected the SiC content of DC and PRP coatings. PRP combined with anionic surfactant to produce an electrophoretic nanoparticle delivery mechanism increasing the SiC content of coatings compared to DC coatings. Higher SiC content was observed at shorter cathodic cycle times.

Keywords: Electrodeposition, nanoparticles, pulse reverse plating codeposition mechanisms, pulse reverse plating, surfactants.

1 Introduction

1.1 Nanocomposite coatings

In recent years there has been a growing interest in the production of electrodeposited nano-composite coatings. There have been a number of reviews [1-4] on the subject and these give a good overview of the diversity of techniques, chemistry and success achieved by researchers in what continues to be an energetic field of research. Such is the interest in this topic that the more recent reviews have tended to focus on specific regions within it; Ni composites [5-11], Ni-Fe alloy composites [12, 13], Ni-Co alloy composites [14, 15], Ni-P composites [16], Ni-B composites [17], Co composites [18] as well as a raft of other papers covering Cu, Zn and Sn which are too numerous to detail here. Electrodeposited metal matrix nanocomposites (MMNCs) have been shown to display improved properties over metal or alloy coatings [19-24] particularly in the areas of tribology [4, 25-29] and corrosion resistance [30-32]. Further to this, models have been published describing the transport and loose adsorption of particles to the working electrode followed by strong adsorption and encapsulation by the growing coating [3, 33-39]. These models have been reviewed fully in literature elsewhere [2] and have highlighted their "failure to quantitatively describe the effect of operational variables, such as current density and electrolyte flow, on deposit particle loading". Due to the lack of complete understanding of the mechanisms utilised, there is currently a significant absence of generic rules and 'standard operating procedures' to design and build a plating bath to allow the deposition of a nanocomposite coating with controllable composition and dispersion, despite the vast amount of research previously done.

1.2 Bath Composition and Parameters

Successful co-electrodeposition of nanoparticles in a metallic matrix is not trivial and is influenced by the plating bath chemistry (particularly the bath additions such as surfactants, levellers and brighteners), the characteristics of the nanoparticles being incorporated, agitation

and operating conditions (including current density and form). Particle composition and size have been shown to have a large effect on codeposition, as this has a direct effect on the ability to make and sustain a good dispersion of particles throughout the electrolyte during deposition. It is widely regarded that particles must possess a sufficiently high zeta potential to maintain a dispersion and prevent agglomeration [20, 21, 40, 41]. This may be significantly affected by addition of a suitable surfactant [21]. A surfactant possessing a charge will surround a nanoparticle, with the hydrophobic carbon-chain tail adsorbing to the particle surface and the hydrophilic charged head facing outwards into solution. Investigators have shown that the addition of a cationic surfactant can help attract particles to the working electrode during DC plating and aid codeposition [21]. In previous work [42], the author established the beneficial effect of combining a cationic surfactant with ultrasonic agitation to produce well dispersed Co-WS_2 nanocomposite coatings, but recognised that cationic surfactants can hinder the cobalt reduction process resulting in codeposition of significant quantities of oxide/hydroxide and a brittle, weakly bonded coating. In the same work, it was shown that a combination of anionic surfactant with a modulated PRP current allowed production and control over particle content within well dispersed nanocomposite coatings. PRP itself is not a new phenomenon, however the method explored here employs long pulses of anodic and cathodic current in the tens of seconds. This low frequency regime of PRP has only been sporadically investigated[43-46]. The ability of PRP to produce high particle content coatings by PRP has been observed by others[43, 46] who claimed the increase in particle density was due to retention of adsorbed particles in the anodic step which were then reincorporated in the matrix during the cathodic cycle. An anodic-electrophoretic component was not recognised. In Weston's work[42] the principle of and anodic-electrophoretic contribution to particle incorporation was founded but not explored in depth.

The technique works by attracting negatively charged nanoparticles to the working electrode during the anodic phase, concentrating the near-electrode region with particles and metal ions

from anodic dissolution. Following this, during the cathodic phase these particles are entrapped within the metal matrix. Particle contents of 4.7-18 vol.% WS_2 were achieved depending on the PRP conditions utilised compared to < 1 vol.% achieved under DC conditions. It was suggested that the technique may be generic, allowing codeposition of a range of nanoparticles from a range of plating baths. If this is the case then a question is raised concerning the role of the anionic surfactant: can the number of particles attracted to the near electrode region be increased in the anodic step (therefore incorporating more nanoparticles in the coating) by increasing the concentration of the surfactant and therefore making the nanoparticles increasingly negatively charged?

1.3 Aims

The main aim of the current work is to demonstrate control of the nSiC content within Co-nSiC coatings produced by PRP by varying the anionic surfactant content of a Co-nSiC plating bath. The change in particle compared to the previous work serves two purposes. Firstly, to investigate the flexibility of the technique by adapting PRP to a new particle material. Secondly, SiC nanoparticles have been proven to disperse readily in the chosen Co-gluconate plating bath, whereas WS_2 do not, hence the effect of anionic surfactant on particle content of coatings produced by PRP can be compared to a baseline series of coatings produced without surfactant.

A further aim of this work is to make uniform coatings which possess enhanced characteristics due to the inclusion of well-dispersed nanoparticles. To investigate this, SEM, EDX and hardness tests were performed to compare the coatings produced by DC plating and PRP.

The PRP technique requires both cathodic and anodic current steps. During anodic steps, insoluble metal hydroxides can form at the electrode surface causing layering and poor adhesion, therefore the speciation of the bath is also of great interest, particularly the likelihood of hydroxide formation. Hence, a final aim of this work is to use speciation models for the bath,

calculated using speciation simulation software, with the aim of establishing a working region of pH where hydroxide formation can be avoided.

2. Experimental Details

2.1 Bath Composition for Deposition Experiments

The composition of baths which have been investigated are given in table 1. The bath chemistry has been used extensively by the authors and characterisation of its behaviour in terms of efficiency and coating characteristics can be seen elsewhere to avoid repetition [42, 47, 48]. For this reason, this paper is concerned with the effect of PRP and anionic surfactant on the composition of coatings produced. All baths were prepared by combining all chemicals in a volumetric flask and adding deionised water from an Elga Purelab Option water purifier to make up one litre of solution. All chemicals were ACS grade supplied by Alfa Aesar and baths were adjusted to pH 6 by correcting with 1M sodium hydroxide. All baths contained 0.25 M cobalt sulphate heptahydrate with sodium D-gluconate (0.5 M) added as a complexant for the cobalt. Sodium chloride was added to enhance conductivity and boric acid was present as a buffer. The bath was split into 100 mL aliquots and to a series of these an anionic surfactant, sodium dodecyl sulphate (SDS), was added to produce baths with 0, 0.2, 0.4, 0.6, 0.8 and 1.0 g L^{-1} SDS. Finally, the silicon carbide nanoparticles (50±5 nm in diameter) supplied by Alfa Aesar were introduced at a concentration of 5 g L^{-1} into each bath and then the ultrasonic probe (Fisher 20 kHz Sonicator CL-334 Ultrasound Probe) operating at 20 W was used to break down the agglomerated particles to form an effective dispersion in solution. The dispersions were stirred with a magnetic follower at 200 rpm during ultrasonic processing.

2.2 Electrodeposition of Coatings

From each bath a series of electrodeposited coatings was produced using direct current (DC) and the pulse reverse plating (PRP) technique. In all cases the working electrode was a 5 x 10 mm mild steel shim cut from Hull cell panels sourced from Schloetter and spot welded to a 0.5

mm diameter NiCr wire. Prior to plating the working electrodes were etched in concentrated nitric acid for 5 s and washed in 10% (w/v) hydrochloric acid and deionised water prior to deposition. In all experiments a cobalt counter electrode of similar dimensions was employed. The reference electrode was a Ag/AgCl sat. KCl. All experiments employed an Autolab potentiostat (Metrohm) running NOVA 2.1 software. The DC sample was plated at 4 A dm^{-2} for 3600 s with bath agitation by an electromagnetic stirrer and the ultrasonic probe continued to operate at 20 W to maintain the dispersion. Pulse reverse (PRP) deposition experiments were conducted upon all baths. In these experiments, the anodic pulse time, t_a, was 10 s, the anodic current density, i_a, was 8 A dm^{-2} and the cathodic current density, i_c, was 4 A dm^{-2}. The cathodic pulse times, t_c, were 30, 40, 60, 90 120 and 240 s and the number of cycles in each experiment were 120, 90, 60 40 30 and 15 respectively. Thus, the total time of held cathodic current amounted to 3600 s in each experiment. Throughout PRP, bath agitation was carried out by an electromagnetic stirrer and the ultrasonic (US) probe which continued to operate at 20 W to maintain the dispersion. In all experiments the temperature was controlled at 80 ± 1 °C by use of a water bath. The surface tension of baths with and without SDS and particles was measured using the Wilhelmy plate method with a Krüss K9 force tensiometer.

2.3 Characterisation

Samples were cut in half and mounted in cross section in Conducto-mount conductive resin (MetPrep) before grinding polishing to a 1 μm diamond finish. All grinding and polishing operations were lubricated with methylated spirits to avoid corrosion. All coatings were examined in cross section in a Philips XL30 scanning electron microscope fitted with a field emission gun (ESEM FEG) and energy dispersive X-Ray (EDX) analyser. EDX was performed for Si(K) and Co(K) across the cross sections on areas measuring 100 μm in length and as wide as allowed by the thickness of the coating. From the EDX results, the volume percent of SiC was calculated from density. Five readings were taken and an average value calculated. The outside edge of each sample was significantly thicker than the centre due to edge effects.

Consequently, the outside 1mm of each sample was ignored as unrepresentative during EDX. Coatings were also subjected microhardness measurements with a LECO-400 Knoop indenter under a 10 gf load for 10 s. Eight measurements were made on each of the deposits in cross section and an average reported.

2.4 Speciation Modelling

The speciation plots were calculated using HYSS 2009 software using similar data to Rudnik [49] compiled from similar sources.

3. Results

3.1 Bath Speciation

A plot of speciation for the bath chemistry is shown in figure 1. The graph shows that $Co(OH)_2$ is unstable at pH below 7.6. The plot shows that at pH 6 the main species in the bath are the aqueous $CoSO_4$ ($[CoSO_4(H_2O)_5]$) and a $CoH_{-1}gluc_3^{2-}$ ($[Cogluc_3]^{2-}$) species. At higher pH the $CoH_{-2}gluc_3^{3-}$ ($[Cogluc_3]^{3-}$) dominates, however as pH increases from approximately pH 7.5 $Co(OH)_2$ begins to form and layering would occur. It is important to keep the solution mildly acidic to prevent hydroxide production, however if the pH is too low the anionic surfactant is protonated by the excess of H^+ ions present, neutralising the charge on the surfactant and thus "turning off" the electrophoretic effect. The speciation of this bath therefore shows that pH 6 is an optimal working pH for this work.

3.2 Coating appearance

In all plating baths the particles dispersed well with the application of stirring and ultrasonic agitation. All coatings produced were of a matt grey appearance. Some coatings had whiskers forming at the edge of the sample due to current edge effects therefore the edges were not included in characterisation.

3.3 Scanning Electron Microscopy

SEM images of all DC coating cross sections in back-scattered electron (BSE) mode are shown in figure 2. All coatings contain a dispersion of nanoparticles however the particle content of each coating varies according to SDS content. The nanoparticles are well dispersed in all coatings with 0-0.8 g L^{-1} SDS, however all show larger more intensely dark black spots and this is particularly noticeable at 0 SDS indicating clusters of nanoparticles. There appears to be an increase in particle content at 0.2 and 0.4 g L^{-1} SDS compared to 0 SDS, however the samples with 0.6, 0.8 and 1.0 g L^{-1} contain progressively fewer particles. The coatings are progressively thinner from 0-0.8 g L-1 SDS but at 1.0 g L^{-1} this is reversed. This corresponds with a change in appearance with vertical cracks opening in the growth direction at high SDS content $\geq$ 0.8 g L^{-1}. These cracks appear to be filled with clusters of nanoparticles. Cross sections of coatings produced by PRP with tc = 60s and variable SDS content are shown in figure 3. Here, similar trends in particle content, thickness and appearance to that seen in DC coating was noted. The difference here is particle content appears to increase with increased SDS content up to 0.6 g L^{-1} and decrease thereafter. Some clusters of nanoparticles still occur. Figure 4 shows Scanning Electron Micrographs in BSE mode of coatings produced from bath containing 0.6 gl^{-1} SDS by PRP with variable cathodic time. Coatings appear to be thinner and contain more particles at lower tc. Also at tc < 90 s, interfacial adhesion is poor attributed to pitting of the mild steel in early anodic cycles. Figure 5a shows a low magnification SEM/BSE image of the coating produced from a bath containing 0.4 g L^{-1} SDS under PRP conditions with a cathodic time t_c = 60 s. Figures 5b-d show a higher magnification image of the same sample in the centre of the coating at different accelerating voltages. These images are of a typical coating and are presented so that the reader may observe how the nanoparticles are distributed in the coating. While it is not very clear, there is a possibility that there is evidence of layering of particles occurring. In all cases except 0 g L^{-1} SDS, the particle content appears higher at low t_c. The SiC volume fraction expressed as a percentage was calculated from EDX results and is shown in Figure 6a and 6b plotted against t_c for the baths with different SDS content. Figure 6a shows

particle content of coatings from baths with 0-0.6 g L-1 plotted against cathodic time. With 0 SDS the particle content of the coating is similar, 6-7 vol.% at all values of t_c. Addition of SDS to the bath at 0.2 g L^{-1} increases the particle content of the coating with higher particle content at lower t_c. The general trend is that increasing the SDS content up to 0.6 g L^{-1} gives increased particle content and higher particle contents are strongly associated with shorter cathodic time t_c, i.e. a higher pulse frequency gives more nano particles when SDS is present. Addition of more SDS to 0.8 and 1.0 g L^{-1} decreases the fraction of particles in the coating however shorter t_c still gives an increased particle content over the bath with 0 SDS. At 1.0 g L^{-1} SDS the particle content of the coating is lower than the 0 SDS bath at $t_c \geq 60$ s.

3.4 Hardness

The Knoop hardness results are seen in figure 7 plotted against particle content of the coatings. There is no obvious relationship between hardness and particle content however there does appear to be a maximum hardness of around 600 kgf mm^{-2} at around 9 vol.% SiC.

4. Discussion

4.1 Speciation

The pulse reverse plating technique is based on 2 bath design principles:

1. The particles possess a negative ζ potential which is conferred by an anionic surfactant.
2. The bath chemistry is designed so that formed metal ions do not form hydroxides in the anodic step.

These are key to producing a coating which does not exhibit layering, where insoluble hydroxide is formed during the anodic step, forming a barrier between consecutive layers of metal deposited in the cathodic step. Hence for PRP to work we need to produce a bath chemistry which destabilises cobalt hydroxide at the pH utilised. Figure 1 shows that cobalt hydroxide is predicted to be unstable at the bath operating pH 6 this is confirmed by the

chemicals used in preparation of the bath readily dissolving on preparation and subsequent pH adjustments to pH 6 by addition of 1 M sodium hydroxide solution. These models are not perfect and to check the validity the bath pH was adjusted to 13 by incremental edition of sodium hydroxide without any visible sign of precipitation i.e. the predicted formation of cobalt hydroxide above pH 7.6 was not observed.

4.2 The Effect of SDS Content on Particle Codeposition

The cross sections of coatings made under DC conditions shown in figure 2 reveal that the addition of SDS reduces the thickness of the coating from 0.2-0.8 g L^{-1} SDS which is attributed to a drop in cathode efficiency however at 1.0 g L^{-1} SDS a thicker coating is deposited.

The n-SiC particle content of the DC coatings is shown in figure 8 which is a plot of particle content versus SDS content for coatings produced under DC and PRP conditions. Of interest here is the increase in n-SiC content with 0.2 g L^{-1} SDS compared to 0 SDS. With subsequent addition of 0.4-1.0 g L-1 SDS the particle content decreases steadily. Under DC conditions, the initial increase in n-SiC content with addition of SDS is attributed to a better dispersion of nanoparticles in the plating path during the deposition process. The subsequent decrease below 0 SDS levels, in n-SiC content from 0.6-1.0 g L^{-1} SDS can be attributed to the saturation of the available particle surface area with SDS molecules and subsequent micelle formation in the bath which then caused particles to agglomerate. This argument may be supported by a simple calculation comparing the molecular area covered by different concentrations of SDS and comparing that with the surface area of the nano particles. The 50 nm n-SiC nanoparticles are approximately spherical and have a total surface area of ~190 m^2 at 5 g L^{-1}. Table 2 shows the total surface area covered at different SDS concentrations assuming SDS has a molecular area of 0.40 x 10^{-18} m^2 [50]. The areas are of a similar order. The SDS in the bath is in equilibrium between three states: free molecules, micelles and molecules adsorbed to nanoparticles. Other surfaces are also covered but are trivially small in comparison to the nanoparticles surface area.

Figure 9 shows the surface tension of the bath with and without particles. All concentrations of SDS in the range 0.1-1.0 g L^{-1} are above critical micelle concentrations. The three-way equilibrium proposed for the nanoparticle bath is reasonable and given the similarity in area of coverage with total particle surface area, it is reasonable to conclude that SDS molecules titrate onto the surface of particles until the surface is saturated at which point the micelle formation dominates.

Figure 8 also shows the effect of SDS content on coatings produced by PRP. Here data is presented with similar cathodic time. In each case, adding SDS increases particle content of the coating up to 0.6 g L^{-1} and thereafter decreases. The initial increase in particle content is attributed to the titration of SDS onto the particle surface which increases the negative ζ potential on the particles. Similar effects have been shown by other workers [40]. The effect of increasing hexadecylpyridinium bromide (HPB) surfactant on Ni-Al_2O_3 coatings was explored by Zhang [40]. They showed an increase in negative ζ potential followed by a levelling off which was accompanied by a similar pattern in particle content of the coatings. We assume that this behaviour is caused by a similar saturation of the surface of the nano particles with adsorbed surfactant. Other researchers have seen similar effects such as Mohajeri et al [51]. The increase in particle content with increased SDS content in PRP is of some significance. It was observed that this increase in SDS did have a small increase on particle content in the DC case which was attributed to an improved dispersion of nanoparticles in the plating bath with more negative ζ potential. When PRP is employed the particle content of coatings with SDS is significantly increased as seen in figure 3 and plotted in figures 6 and 8. This implies that increasing SDS increases the negative ζ potential of nano particles which attracts more nano particles to the working electrode during the anodic step and increases the probability of particle adsorption and subsequent encapsulation in the cathodic step. Once the surface area of the nano particles has saturated with adsorbed SDS molecules subsequent SDS additions serve to increase micelle formation. Since these are effectively high charge density nanoparticles they will compete with

SiC nano particles at the working electrode surface and hence fewer of these particles are encapsulated in the cathodic step. The result of this is that there is an optimum SDS content of the bath which promotes particle codeposition by PRP. in our previous work [47] we saw similar effects for SDS on Al_2O_3 of similar diameter in the same bath chemistry. In that case the optimum SDS content was 0.4 g L^{-1} whereas here it is 0.6 g L^{-1}. Furthermore, the effectiveness of SDS and PRP is far higher for SiC then for Al_2O_3 which we attribute to differing ζ potentials of the different particles. In previous work, we established a model which describes the whole PRP process. The current work expands on our theoretical model and is explored here so that we might move towards a generic technique which may be applied to other systems.

4.3 The Pulse Reverse Plating Codeposition Mechanism

During the anodic step increased SDS content gives more negative ζ potential and leads to more particles being adsorbed and increased particle encapsulation. PRP combined with SDS is therefore a delivery mechanism of nanoparticles to the working electrode in the anodic step.

This delivery mechanism is responsive to increases in SDS content until such point that the surface area of the nanoparticles is saturated. After this point the micelles compete with nanoparticles at the surface of the working electrode so fewer particles are encapsulated. The use of variable SDS content in this work shows the significant effect of SDS and ζ potential on the electrophoretic attraction of particles to the working electrode, their adsorption and subsequent encapsulation. The whole process is described schematically in figure 10. Figure 10a shows particles dispersed in the electrolyte surrounded by an associated cloud of adsorbed ions. This is similar to the ideas proposed by Buelens et al [34]. The anodic working electrode attracts these particles towards it. At the same time Co^{2+} ions are produced and pass into solution increasing their concentration close to the electrode surface. Over the course of the anodic pulse the concentration of particles at and near the surface will increase. The force attracting the

particle to the working electrode will be proportional to the charge on the particle and hence directly related to the concentration of SDS in the plating bath. This is limited by the finite surface area of the particles. As the particle and associated ion cloud come into close proximity to the anode, figure 10b, the cloud is likely to undergo change as local chemistry and charge effects occur. The presence of adsorbed Co^{2+} ions may increase due to increased Co^{2+} concentration close to the anode. The ionic cloud of the particle also contains SDS molecules and these are strongly attracted to the anode, hence the particle is drawn into a region close to the electrode which is rich in Co^{2+} ions and SDS, figure 10c. During the anodic step, the nature of the working electrode surface is a place of great interest.

The interaction of SDS with the surface is dependent on the concentration. The model proposed by Arnebrant [52] for SDS on chromium consists of a low concentration adsorption consisting of well dispersed SDS molecules adsorbed by either the hydrophilic head and or the hydrophobic tail, an intermediate concentration region in which a broken monolayer of SDS molecules are adsorbed on the Cr surface via the anionic head with aligned hydrophobic tails, and a high concentration region which occurs above critical micelle concentration (CMC) and consists of a bilayer of highly ordered SDS molecules. Our measurement of surface tension indicated that all our baths were above CMC, however we must also take into account that we have a large surface area of nano particles present and that may have some effect on the reliability of a neat bilayer model. Factors also disrupting the absorbed SDS layer are the constant production of Co^{2+} ions and the ultrasonic agitation employed during the plating process. The concentration of SDS in this work varies from ~0.7-3.5 mM which is low compared to the CMC of SDS in water, 8.25 mM [52, 53]. However, CMC is greatly reduced in the presence of high ionic concentration [53, 54] and particularly in the presence of Co^{2+} ions. Given the combination of factors affecting the surface of the working electrode it is reasonable to assume a single disrupted monolayer such as Arnebrant described as an intermediate case. This is shown schematically in figure 10a-c. Lokar [55] proposed a

thermodynamic model for the strength of adhesion between a particle in aqueous surfactant solution and a flat solid. The model describes an energy minimum with the particle in close proximity to the surface, while maintaining a very thin film of surfactant between the two. In the anodic step the inter surface region between nanoparticle and working electrode is also filled with Co^{2+} ions. Some of these may be considered to be part of the cloud of ions surrounding the nanoparticle. As Paria [56] noted, an electrolyte that "salts out" a surfactant will promote adsorption. The presence of continuous Co^{2+} at the anode may therefore promote selective adsorption of SDS at the anode. These effects combined to produce an ideal situation for promoting particle and encapsulation on switching to cathodic mode. At the beginning of the cathodic phase, two effects occur immediately:

1. Co^{2+} ions associated with the ionic cloud are reduced.
2. SDS is repelled from the surface of the cathode.

These effects are depicted in figure 10d. As the cathodic cycle progresses, the concentration of nano particles at the surface will decrease due to encapsulation and diffusion while an equilibrium flux of particles to and from the surface similar to that in DC is attained. At some point another anodic pulse is required to increase particle concentration and adsorption. The higher the pulse frequency, the more particles will be incorporated into the growing coating. The model described predicts a controllable system for delivery and capture of nanoparticles at a growing electrodeposited metallic matrix. Each anodic pulse provides a boost to nanoparticle content in the coating. It has been shown that the bath efficiency varies with shorter t_c giving higher efficiency. Figure 10e shows a schematic of the anodic process at high SDS concentration. The particles now compete at the electrode surface with micelles and excess SDS molecules adsorbed on the anode surface. This suppresses adsorption and encapsulation of nanoparticles.

4.4 The PRP/SDS Boost

The work presented shows that adding SDS to the plating bath and applying PRP improves significantly the quantity and dispersion of nanoparticles in the coatings produced. During DC deposition all baths produced a nanocomposite coating. This is assumed to be due to random collisions of particles with the cathode and subsequent entrapment in the growing coating. Figure 8 shows the addition of SDS improves the chances of encapsulation in DC conditions, up to 0.6 g L^{-1} but thereafter it decreases. Figure 8 also shows that introducing PRP increases the particle content of coatings, and that the higher the pulse frequency, the higher the particle uptake. The question arises; how many particles are captured per pulse? How do we analyse the effectiveness of pulses in the ability to capture nanoparticles?

To do this, we need to know how the particles are captured throughout cathodic pulse. With 0 g L^{-1} SDS we have seen the particle content of the coating is the same regardless of PRP conditions hence we need to be able to measure the rate of particle capture as the coating grows. This is achieved by expressing the number of particles captured per cycle expressed as a fractional area of coverage of the electrode and plotting that against the thickness of coating deposited per cycle expressed in particle diameters. The resulting graph is shown in Figure 11a.

It is useful to add some points of reference to this graph to give context. If the nanoparticles are considered to be spheres, then the maximum packing density would give a value of $\theta = 0.9069$ to be achieved at a normalised coating thickness of 1. This value is extremely unlikely however, and a more reasonable figure to take might be hcp close packing density of 0.74, however this seems extremely unlikely as there are no bonding forces between particles. In a chaotic, random accumulation of particles at the surface and subsequent capture, an upper maximum of 0.64 seems an appropriate maximum which might be aspired to since it represents the approximate packing density of an amorphous metal. Again, without inter particle bonding this seems an extreme value, but one that helps guide examination of the data. Hence the black solid line in Figure 11a represents this value. The black dotted line with a gradient of 0.64 shows the maximum attainable packing value with growth. Plotting the data for 0 g L^{-1} SDS produces a

straight-line relationship with a line of best fit passing close to the origin which is consistent with the theory that pulsing confers no benefit. With 0 g L^{-1} SDS, a normalised coating thickness of 7.5 is required to achieve $\theta = 0.64$, the line having a gradient of 0.106. The effect of adding SDS on particle capture is that at short t_c, the gradient of each plot shifts towards the ideal gradient. In physical terms, at the beginning of the cathodic pulse, the population of nanoparticles at the surface is high as a consequence of the previous anodic pulse attracting the negatively charged particles. From 0.2-0.6 g L^{-1} SDS this effect is increasingly pronounced. At longer t_c the lines adopt a gradient parallel to the 0 g L^{-1} SDS, and this represents the depletion of nanoparticles close to working electrode, i.e. with longer t_c the boost effect of the previous pulse is lost and the coating comes to resemble a DC produced coating. With higher SDS content 0.8-1.0 g L^{-1} we have already seen that the DC coatings contain fewer particles, hence, although there is a boost in particle content at low t_c, the subsequent transition to DC type behaviour at longer pulses results in fewer particles being captured compared to the 0 g L^{-1} SDS case. Hence, the gradient of these data at higher t_c are much lower. It can now be seen that the pulse increases particle content up to approximately 5 particle diameters before levelling off giving a maximum useful t_c pulse length. It is interesting that all baths with SDS appear to attain a fractional coverage of approximately $\theta = 0.33$ within 2 to 2.5 coating diameters. This indicates that a particle at the surface at the beginning of the cathodic step has approximately 20 to 25% chance of becoming captured by the growing coating. This looks a very good rate of capture to the authors.

Another way to look at the effectiveness of the boost caused by the pulse is to plot the same data but subtract out the DC value for area coverage from each SDS content. Hence 0 g L^{-1} SDS now approximates to a flat line in Figure 11b. Adding 0.2 g L^{-1} SDS gives a boost in the first five diameters, 0.4 g L^{-1} in the first 20 and 0.6 g L^{-1} gives a permanent post over DC under the same conditions. Whatever the SDS content, PRP always gives an improved particle content due to increased particle concentrations near the working electrode during the anodic step

leading to increased probability of adsorption and capture in the cathodic step. Finally, in figure 12 we compare the particle content of the coatings produced with 0.2 g L^{-1} SDS. Here we are starting to see that similar patterns of behaviour are produced from the same bath conditions with different particle size and chemistry. We believe this shows the potential offered by the PRP technique to produce nanocomposite coatings from any bath in which the anodic behaviour is controlled to avoid layering.

4.5 Bath Efficiency.

The efficiency of similar baths were reported previously [47]. In that work the efficiency at DC was 60-75% which improved with shorter t_c. While there is no problem with layering due to $Co(OH)_2$ formation in this or previous work, there remains the possibility that pH can increase near the working electrode during the cathodic step due to the reduction of H^+ ions and that this could lead to layering. Therefore, the effect of complexing agent can have both a positive and negative effect on coatings produced by PRP and a balance between the ability to destabilise the solid hydroxide and the decrease in efficiency, leading to increased pH must be found in future work.

4.6 Effect of pH

We have discussed that increasing pH during PRP is best avoided as it can give layering. A low pH is likely to have a strong effect on ζ potential and compete at the surface of nanoparticles with the anionic surfactant. This predicts an operating pH window which must be explored further for this and other potential systems.

5. Conclusions

In DC plating conditions, adding SDS to a Co-nSiC plating bath up to 0.4 g L^{-1} increases the n-SiC content of coatings, as the more negative potential improves dispersion of the nanoparticles in the plating bath. In additions of more than 0.4 g L^{-1}, a decrease in particle content of

electrodeposited coatings is observed as the surface area of the nanoparticles becomes saturated and the dispersion is destabilised by excessive micelle formation.

In PRP, the use of an anionic surfactant in concentrations of up to 0.6 g L^{-1} promotes particles inclusion when compared to DC plating, due to the electrophoretic attraction of particles to the working electrode in the anodic phase. At SDS content of greater than 0.6 g L^{-1}, the particle content of coatings in decreases as the surface area of the nanoparticles again becomes saturated and the dispersion is destabilised by excessive micelle formation. Without SDS there is no increase in particle content due to PRP. It is clear that the ζ potential of the particles in the bath is of great importance. This should be considered more fully in future work.

The use of shorter cathodic times (t_c) in the period of tens of seconds produces coatings with higher particle content. By varying t_c and SDS content, the particle content of coatings is controllable. By demonstrating these relationships, the combination of PRP with anionic surfactant shows the generic nature of the technique in the chosen cobalt electrolyte. Where previous work hasn't utilised the anodic step to aid nanoparticle inclusion, the method discussed here creates a mechanism for delivering nanoparticles to the working electrode during the anodic phase, which are then encapsulated during the cathodic phase.

In order to develop a generic technique, the bath chemistry to allow electrodeposition of common coatings e.g. Ni or Zn, should be modelled based on similar principles to those presented here, and optimised so that efficiency is maximised and oxide/hydroxides destabilised.

References

[1] F. Walsh, C. Ponce de Leon, A review of the electrodeposition of metal matrix composite coatings by inclusion of particles in a metal layer: an established and diversifying technology, Transactions of the IMF 92(2) (2014) 83-98.

[2] F.C. Walsh, S. Wang, N. Zhou, The electrodeposition of composite coatings: Diversity, applications and challenges, Current Opinion in Electrochemistry 20 (2020) 8-19.

[3] J.L. Stojak, J. Fransaer, J.B. Talbot, Review of electrocodeposition, Advances in Electrochemical Science and Engineering 7 (2002) 193-224.

[4] C. Low, R. Wills, F. Walsh, Electrodeposition of composite coatings containing nanoparticles in a metal deposit, Surface and Coatings Technology 201(1-2) (2006) 371-383.

[5] P. Priyadarshi, P.K. Katiyar, R. Maurya, A review on mechanical, tribological and electrochemical performance of ceramic particle-reinforced Ni-based electrodeposited composite coatings, Journal of Materials Science (2022) 1-33.

[6] M. Sajjadnejad, S.M.S. Haghshenas, P. Badr, N. Setoudeh, S. Hosseinpour, Wear and tribological characterization of nickel matrix electrodeposited composites: A review, Wear 486 (2021) 204098.

[7] Y.H. Ahmad, A. Mohamed, Electrodeposition of nanostructured nickel-ceramic composite coatings: a review, Int. J. Electrochem. Sci., 9, (2014) 1942 - 1963,.

[8] Z. Mahidashti, M. Aliofkhazraei, N. Lotfi, Review of nickel-based electrodeposited tribo-coatings, Transactions of the Indian Institute of Metals 71(2) (2018) 257-295.

[9] A.D. Torkamani, M. Velashjerdi, A. Abbas, M. Bolourchi, P. Maji, Electrodeposition of Nickel matrix composite coatings via various Boride particles: A review, Journal of Composites and Compounds 3(7) (2021) 106-113.

[10] B. Szeptycka, A. Gajewska-Midzialek, T. Babul, Electrodeposition and corrosion resistance of Ni-graphene composite coatings, Journal of Materials Engineering and Performance 25(8) (2016) 3134-3138.

[11] C.R. Raghavendra, S. Basavarajappa, I. Sogalad, Electrodeposition of Ni-nano composite coatings: a review, Inorganic and Nano-Metal Chemistry 48(12) (2018) 583-598.

[12] V. Torabinejad, M. Aliofkhazraei, S. Assareh, M. Allahyarzadeh, A.S. Rouhaghdam, Electrodeposition of Ni-Fe alloys, composites, and nano coatings–A review, Journal of Alloys and Compounds 691 (2017) 841-859.

[13] A.K. Chaudhari, V. Singh, A review of fundamental aspects, characterization and applications of electrodeposited nanocrystalline iron group metals, Ni-Fe alloy and oxide ceramics reinforced nanocomposite coatings, Journal of Alloys and Compounds 751 (2018) 194-214.

[14] M.S. Safavi, M. Tanhaei, M.F. Ahmadipour, R.G. Adli, S. Mahdavi, F.C. Walsh, Electrodeposited Ni-Co alloy-particle composite coatings: a comprehensive review, Surface and Coatings Technology 382 (2020) 125153.

[15] A. Karimzadeh, M. Aliofkhazraei, F.C. Walsh, A review of electrodeposited Ni-Co alloy and composite coatings: Microstructure, properties and applications, Surface and Coatings Technology 372 (2019) 463-498.

[16] A. Lelevic, F.C. Walsh, Electrodeposition of NiP alloy coatings: a review, Surface and Coatings Technology 369 (2019) 198-220.

[17] E. Ünal, A. Yaşar, İ.H. Karahan, A review of electrodeposited composite coatings with Ni–B alloy matrix, Materials Research Express 6(9) (2019) 092004.

[18] A. Rahman, M.A. Chowdhury, N. Hossain, M. Rana, M.J. Alam, A review of the tribological behavior of electrodeposited cobalt (Co) based composite coatings, Composites Part C: Open Access (2022) 100307.

[19] C.T.J. Low, R.G.A. Wills, F.C. Walsh, Electrodeposition of composite coatings containing nanoparticles in a metal deposit, Surf. Coat. Technol. 201(1-2) (2006) 371-383.

[20] S.C. Wang, W.C.J. Wei, Kinetics of electroplating process of nano-sized ceramic particle/Ni composite, Materials Chemistry and Physics 78(3) (2003) 574-580.

[21] M.D. Ger, Electrochemical deposition of nickel/SiC composites in the presence of surfactants, Materials Chemistry and Physics 87(1) (2004) 67-74.

[22] H.K. Lee, H.Y. Lee, J.M. Jeon, Codeposition of micro- and nano-sized SiC particles in the nickel matrix composite coatings obtained by electroplating, Surf. Coat. Technol. 201(8) (2007) 4711-4717.

[23] G. Wu, N. Li, D.R. Zhou, K. Mitsuo, Electrodeposited Co-Ni-Al2O3 composite coatings, Surf. Coat. Technol. 176(2) (2004) 157-164.

[24] L. Chen, L.P. Wang, Z.X. Zeng, J.Y. Zhang, Effect of surfactant on the electrodeposition and wear resistance of Ni-Al2O3 composite coatings, Mater. Sci. Eng. A-Struct. Mater. Prop. Microstruct. Process. 434(1-2) (2006) 319-325.

[25] M. Sajjadnejad, S.M.S. Haghshenas, V. Tavakoli Targhi, N. Setoudeh, A. Hadipour, A. Moghanian, S. Hosseinpour, Wear behavior of alkaline pulsed electrodeposited nickel composite coatings reinforced by ZnO nanoparticles, Wear 468-469 (2021) 203591.

[26] C.T.J. Low, R.G.A. Wills, F.C. Walsh, Electrodeposition of composite coatings containing nanoparticles in a metal deposit, Surface and Coatings Technology 201(1-2) (2006) 371-383.

[27] S. Pinate, P. Leisner, C. Zanella, Wear resistance and self-lubrication of electrodeposited Ni-SiC:MoS2 mixed particles composite coatings, Surface and Coatings Technology 421 (2021) 127400.

[28] X. Li, Q. Shen, Y. Zhang, L. Wang, C. Nie, Wear behavior of electrodeposited nickel/graphene composite coating, Diamond and Related Materials 119 (2021) 108589.

[29] H. Zhang, J. Wang, S. Chen, H. Wang, Y. He, C. Ma, Ni–SiC composite coatings with improved wear and corrosion resistance synthesized via ultrasonic electrodeposition, Ceramics International 47(7, Part A) (2021) 9437-9446.

[30] Y. Zhang, S. Zhang, Y. He, H. Li, T. He, Y. Fan, H. Zhang, Mechanical properties and corrosion resistance of pulse electrodeposited Ni-B/B4C composite coatings, Surface and Coatings Technology 421 (2021) 127458.

[31] C.M.P. Kumar, A. Lakshmikanthan, M.P.G. Chandrashekarappa, D.Y. Pimenov, K. Giasin, Electrodeposition Based Preparation of Zn–Ni Alloy and Zn–Ni–WC Nano-Composite Coatings for Corrosion-Resistant Applications, Coatings 11(6) (2021) 712.

[32] N.P. Wasekar, A.P. O'Mullane, M.A. Sayeed, G. Sundararajan, Influence of SiC reinforcement content and heat treatment on the corrosion behavior of pulsed electrodeposited Ni-W alloy metal matrix composite, Materialia 22 (2022) 101390.

[33] N. Guglielmi, Kinetics of the deposition of inert particles from electrolytic baths, Journal of the Electrochemical Society 119(8) (1972) 1009.

[34] J.-P. Celis, J. Roos, C. Buelens, A mathematical model for the electrolytic codeposition of particles with a metallic matrix, Journal of the Electrochemical Society 134(6) (1987) 1402.

[35] J.-P. Celis, J. Roos, C. Buelens, J. Fransaer, Mechanism of electrolytic composite plating: survey and trends, Transactions of the IMF 69(4) (1991) 133-139.

[36] J. Roos, J.-P. Celis, J. Fransaer, C. Buelens, The development of composite plating for advanced materials, Jom 42(11) (1990) 60-63.

[37] J.L. Valdes, Electrodeposition of colloidal particles, Journal of the Electrochemical Society 134(4) (1987) 223C.

[38] A. Hovestad, L. Janssen, Electrochemical codeposition of inert particles in a metallic matrix, Journal of Applied Electrochemistry 25(6) (1995) 519-527.

[39] B. Łosiewicz, Electrodeposition mechanism of composite coatings, Solid State Phenomena 228 (2015) 65-78.

[40] L. Chen, L. Wang, Z. Zeng, J. Zhang, Effect of surfactant on the electrodeposition and wear resistance of Ni-Al2O3 composite coatings, Materials Science and Engineering A 434(1-2) (2006) 319-325.

[41] H.K. Lee, H.Y. Lee, J.M. Jeon, Codeposition of micro- and nano-sized SiC particles in the nickel matrix composite coatings obtained by electroplating, Surface and Coatings Technology 201(8) (2007) 4711-4717.

[42] D.P. Weston, Y.Q. Zhu, D. Zhang, C. Miller, D.G. Kingerley, C. Carpenter, S.J. Harris, N.J. Weston, Co-electrodeposition of inorganic fullerene (IF-WS2) nano-particles with cobalt from a gluconate bath with anionic and cationic surfactants, Electrochimica Acta 56(19) (2011) 6837-6846.

[43] P. Xiong-Skiba, D. Engelhaupt, R. Hulguin, B. Ramsey, Effect of pulse plating parameters on the composition of alumina/nickel composite, Journal of the Electrochemical Society 152(8) (2005) C571-C576.

[44] A.B. Vidrine, E.J. Podlaha, Composite electrodeposition of ultrafine γ-alumina particles in nickel matrices Part I: Citrate and chloride electrolytes, Journal of Applied Electrochemistry 31(4) (2001) 461-468.

[45] E.J. Podlaha, Selective Electrodeposition of Nanoparticulates into Metal Matrices, Nano Letters 1(8) (2001) 413-416.

[46] E.J. Podlaha, D. Landolt, Pulse-reverse plating of nanocomposite thin films, Journal of the Electrochemical Society 144(7) (1997) L200-L202.

[47] D. Albusalih, S. Gill, D. Weston, F. Altmann, Production of electroplated Co-Al2O3 nanocomposites by pulse reverse plating (PRP) and anionic surfactant, Transactions of the IMF 97(4) (2019) 203-216.

[48] D.P. Weston, S.J. Harris, P.H. Shipway, N.J. Weston, G.N. Yap, Establishing relationships between bath chemistry, electrodeposition and microstructure of Co–W alloy coatings produced from a gluconate bath, Electrochimica Acta 55(20) (2010) 5695-5708.

[49] E. Rudnik, N. Dashbold, Effect of Cl^- and SO_4^{2-} Ions on Electrodeposition of Cobalt from Acidic Gluconate Solutions, Russian Journal of Electrochemistry 55(12) (2019) 1305-1319.

[50] J. Sjöblom, A.M. Blokhus, W.M. Sun, S.E. Friberg, Surfactants and cosurfactants in lamellar liquid crystals and adsorbed on solid surfaces. I. The model system sodium dodecyl

sulfate/butanol or sodium dodecyl sulfate/benzyl alcohol and α-alumina, Journal of Colloid And Interface Science 140(2) (1990) 481-491.

[51] S. Mohajeri, A. Dolati, S. Rezagholibeiki, Electrodeposition of Ni/WC nano composite in sulfate solution, Materials Chemistry and Physics 129(3) (2011) 746-750.

[52] T. Arnebrant, K. Bäckström, B. Jönsson, T. Nylander, An ellipsometry study of ionic surfactant adsorption on chromium surfaces, Journal of Colloid and Interface Science 128(2) (1989) 303-312.

[53] Y. Moroi, K. Motomura, R. Matuura, The critical micelle concentration of sodium dodecyl sulfate-bivalent metal dodecyl sulfate mixtures in aqueous solutions, Journal of Colloid and Interface Science 46(1) (1974) 111-117.

[54] C. Esposito, P. Colicchio, A. Facchiano, R. Ragone, Effect of a Weak Electrolyte on the Critical Micellar Concentration of Sodium Dodecyl Sulfate, Journal of Colloid and Interface Science 200(2) (1998) 310-312.

[55] W.J. Lokar, W.A. Ducker, Approximate prediction of adhesion between two solids immersed in surfactant solution based on adsorption to an isolated solid, Colloids and Surfaces A: Physicochemical and Engineering Aspects 322(1) (2008) 256-260.

[56] S. Paria, K.C. Khilar, A review on experimental studies of surfactant adsorption at the hydrophilic solid–water interface, Advances in Colloid and Interface Science 110(3) (2004) 75-95.

Table 1. Bath composition		
Chemical	**Concentration M**	**Concentration g L^{-1}**
Cobalt sulfate heptahydrate	0.25	80
Boric acid	0.6	40
Sodium chloride	0.5	30
Sodium D-Gluconate	0.55	110

Figure 1: Cobalt plating bath speciation plot, calculated by HYSS software, using data from Rudnik [47] [colour print]

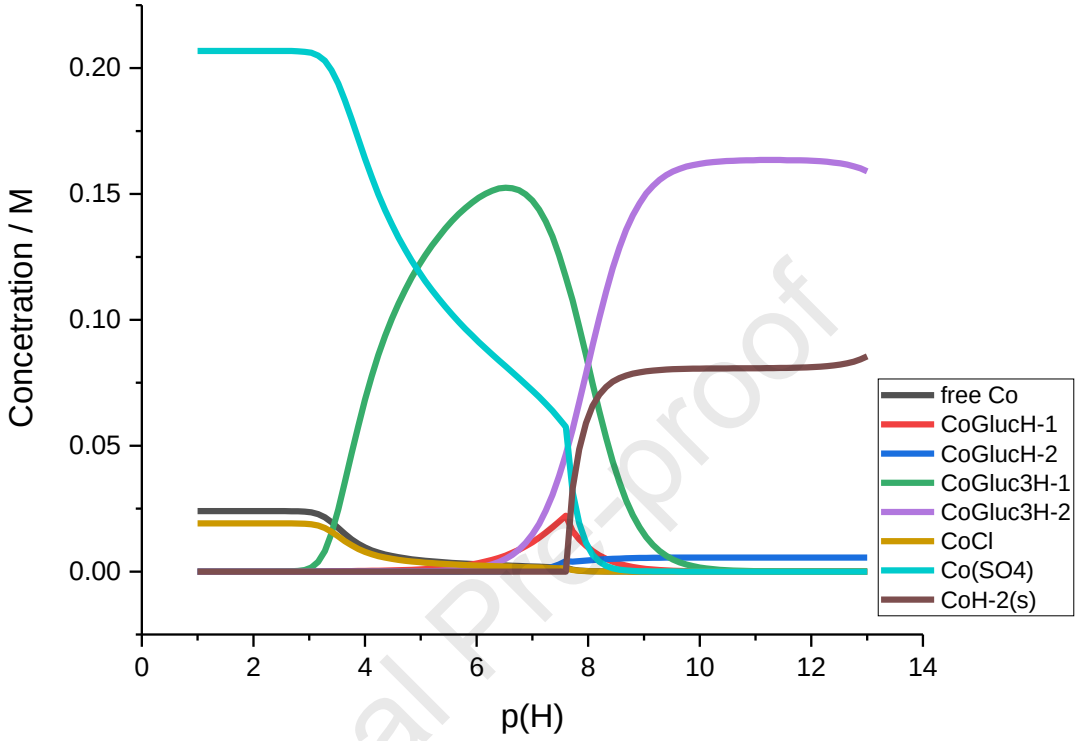

Figure 2: Scanning Electron Micrographs in BSE mode of coatings produced by DC plating from baths with variable SDS content a) 0.0 g L^{-1}, b) 0.2 g L^{-1}, c) 0.4 g L^{-1}, d) 0.6 g L^{-1}, e) 0.8 g L^{-1} and f) 1.0 g L^{-1}.

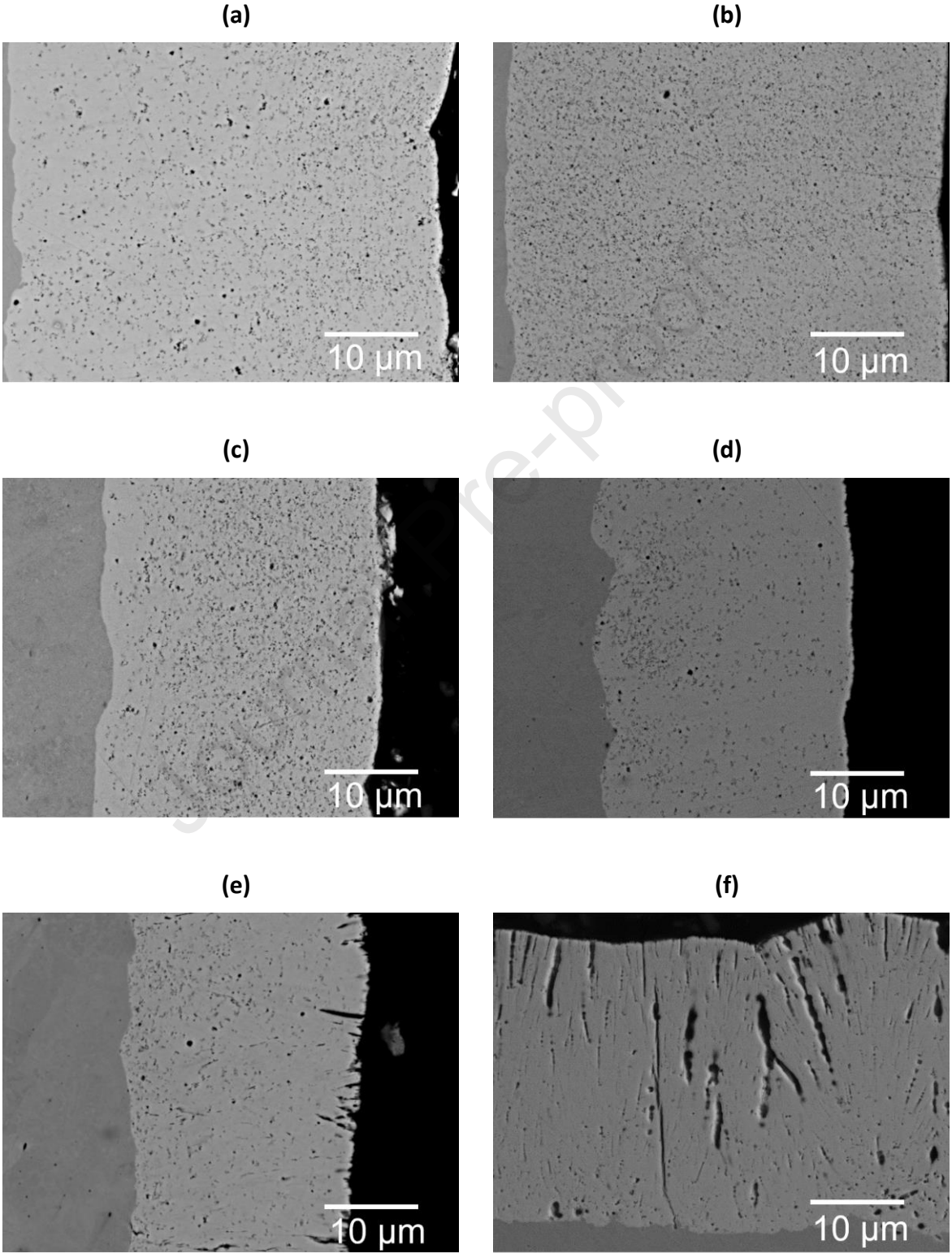

Figure 3: Scanning Electron Micrographs in BSE mode of coatings produced by PRP with tc = 60 s plating from baths with variable SDS content a) 0.0 g L^{-1}, b) 0.2 g L^{-1}, c) 0.4 g L^{-1}, d) 0.6 g L^{-1}, e) 0.8 g L^{-1} and f) 1.0 g L^{-1}.

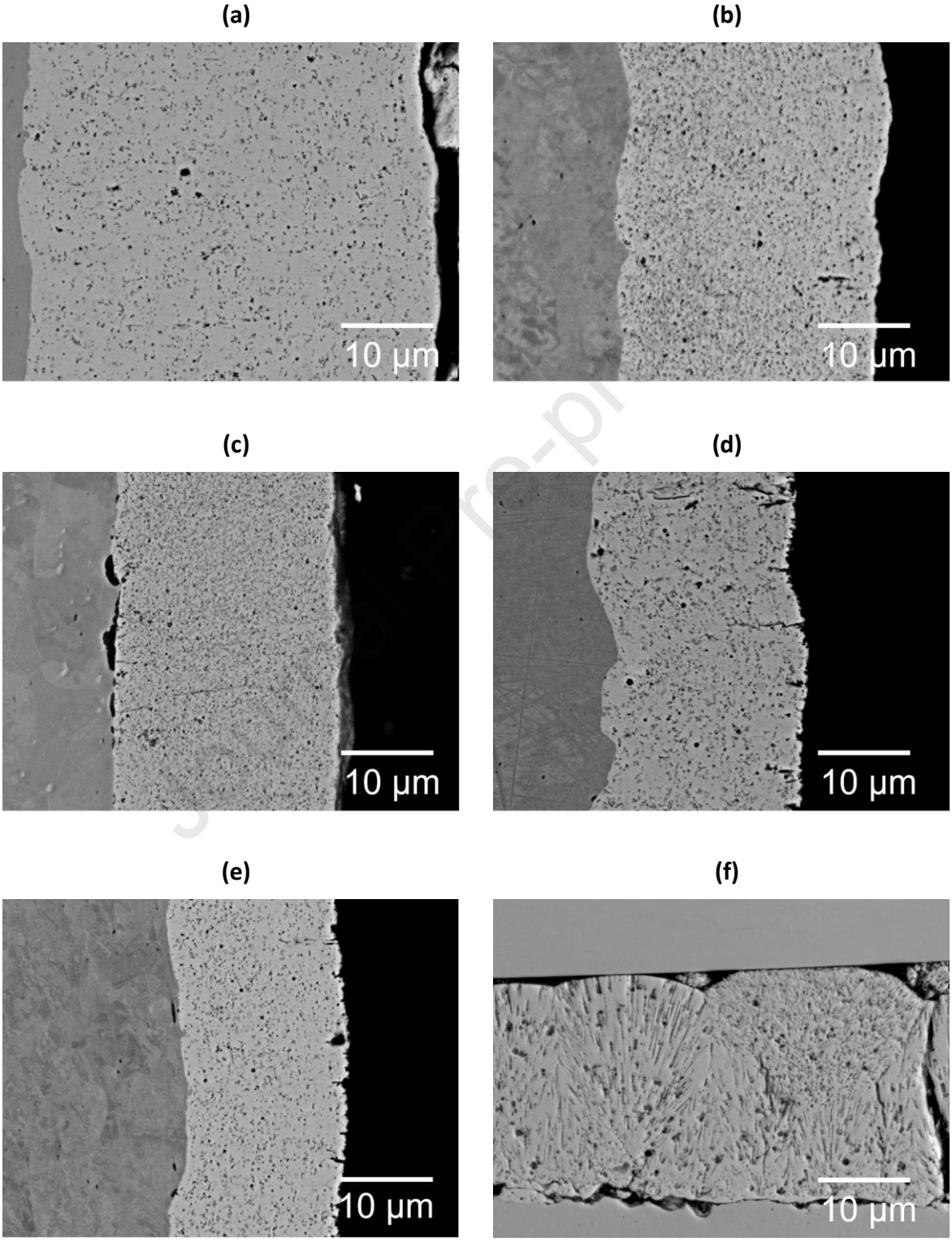

Figure 4: Scanning Electron Micrographs in BSE mode of coatings produced from bath containing 0.6 g L^{-1} SDS by Pulse Reverse Plating (PRP) with variable cathodic time, tc = a) 30 s, b) 40 s, c) 60 s, d) 90 s, e) 120 s and f) 240 s.

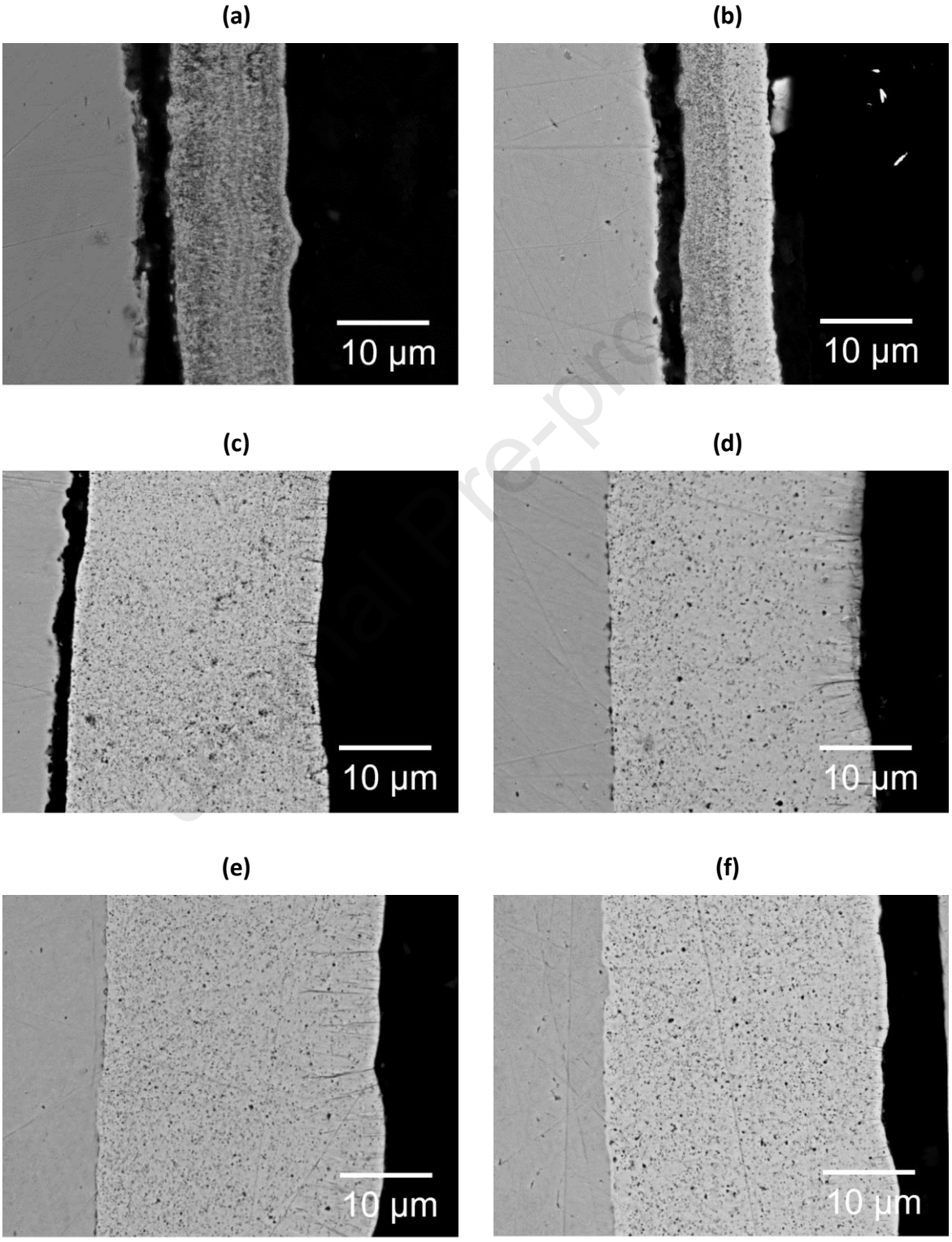

Figure 5: Scanning Electron Micrographs in BSE mode of a coating produced from a bath containing 0.4 g L^{-1} SDS under PRP conditions with a cathodic time t_c = 60 s. a) low magnification b), c) and d) higher magnification images at different accelerating voltage b) 10 kV, c) 15 kV and d) 20 kV. More particles are visible with higher accelerating voltage.

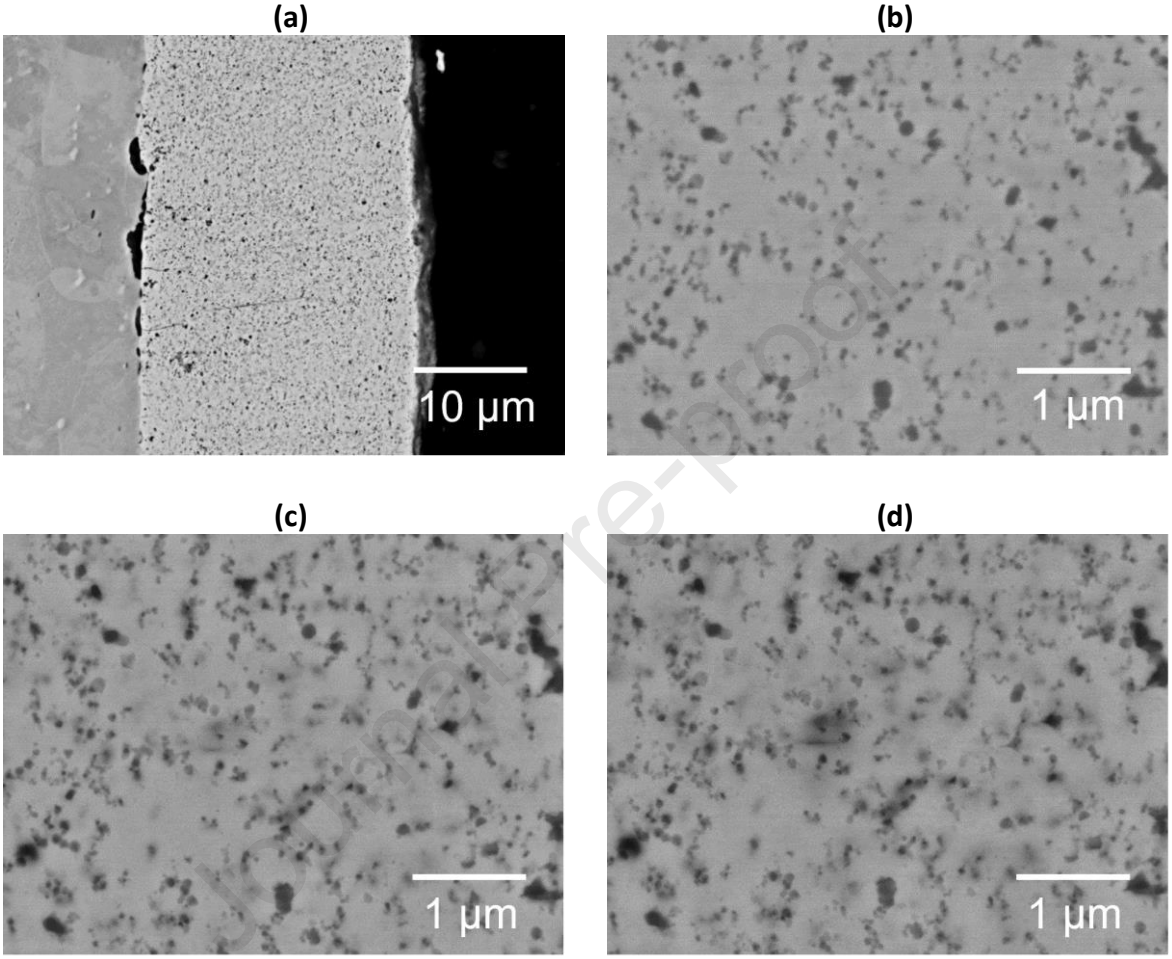

Figure 6: Graphs of particle content in coating versus cathodic time, (t_c) for PRP coatings with SDS content of a) 0, 0.2, 0.4 and 0.6 g L^{-1}, b) depicts coatings with 0.6, 0.8 and 1.0 g L^{-1} SDS. Two graphs are presented for clarity. [colour print]

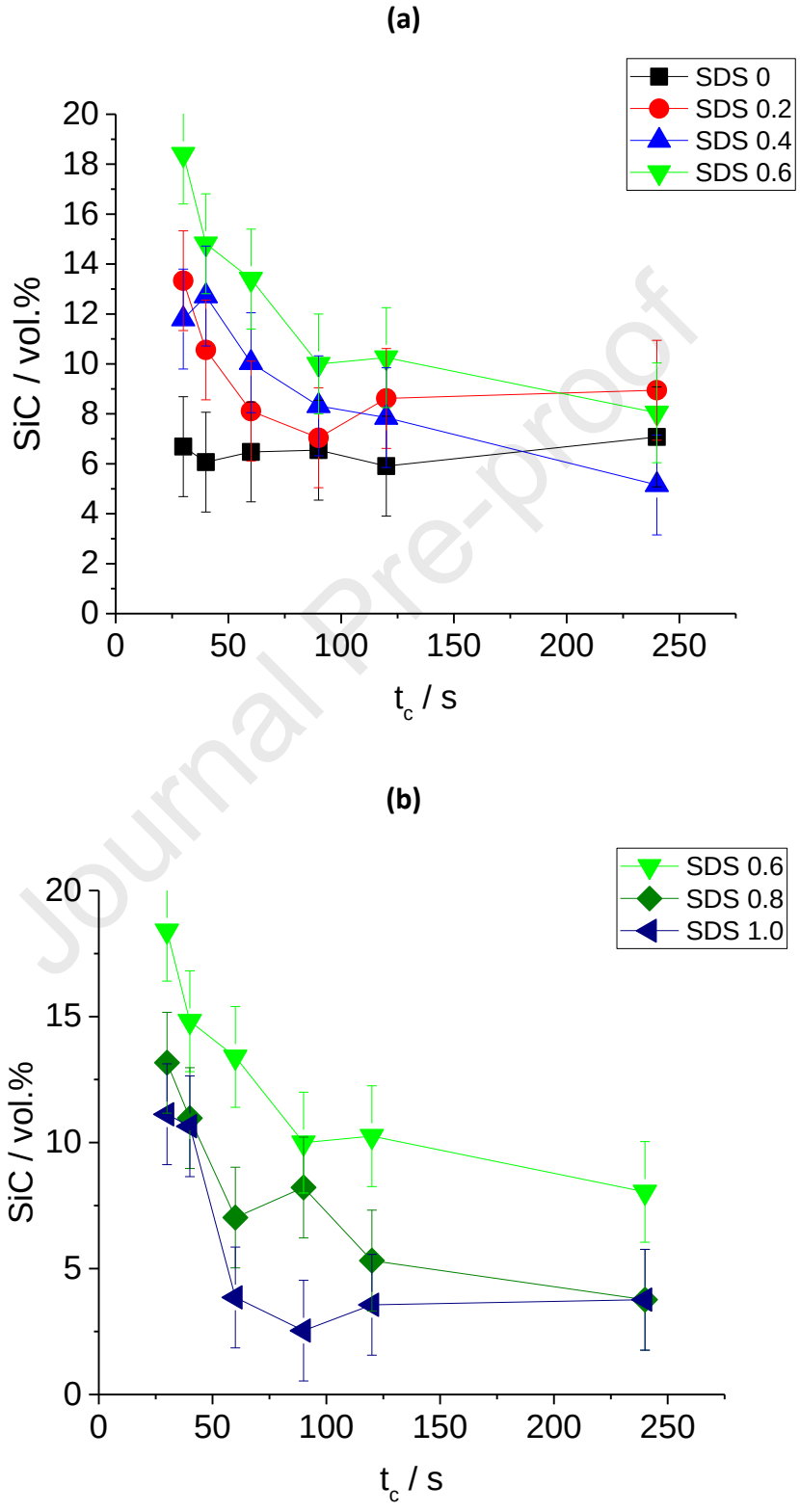

Figure 7: Graph showing Knoop microhardness of Co-SiC coatings with changing SiC nanoparticle content dependent on concentration of SDS used. [colour print]

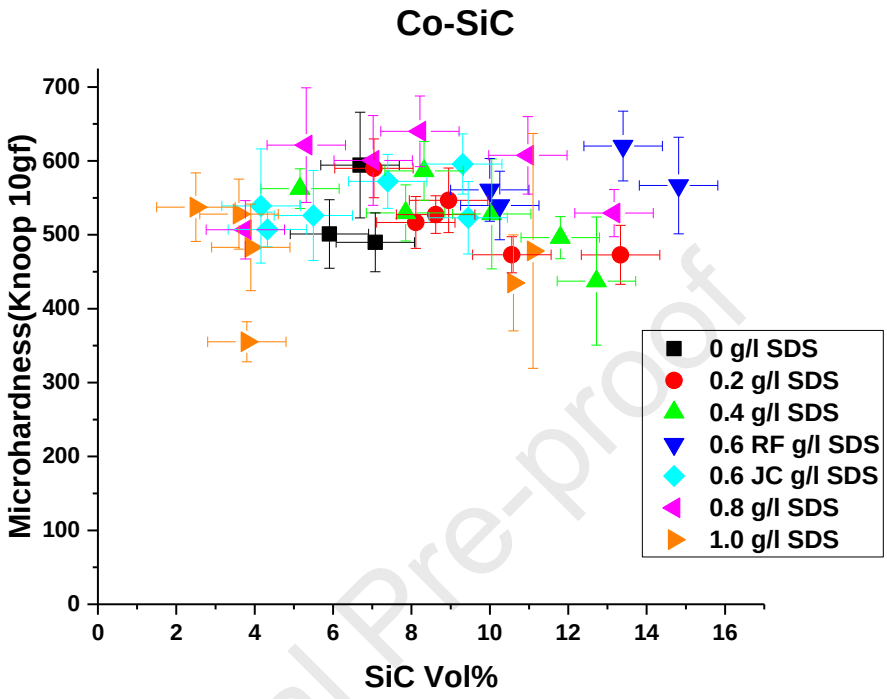

Figure 8: Graph showing the concentration of SiC particles in the cobalt coatings with changing SDS bath concentration, as cathodic time, t_c is varied. [colour print]

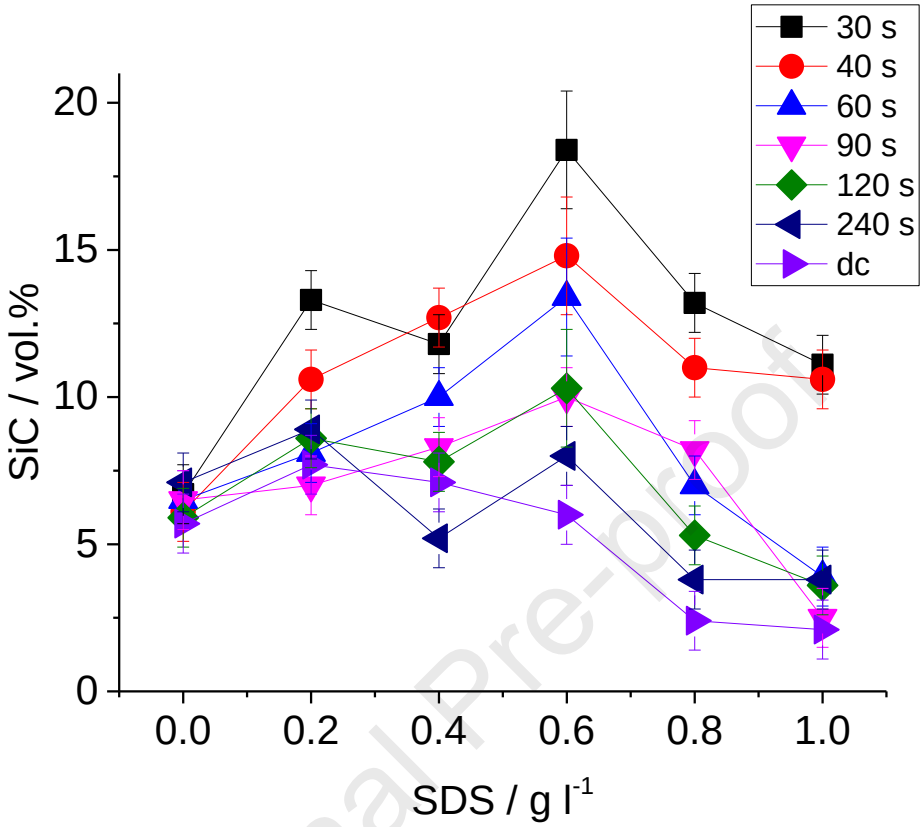

Figure 9: Plating bath surface tension measured with varying SDS content; with and without SiC nanoparticles. [colour print]

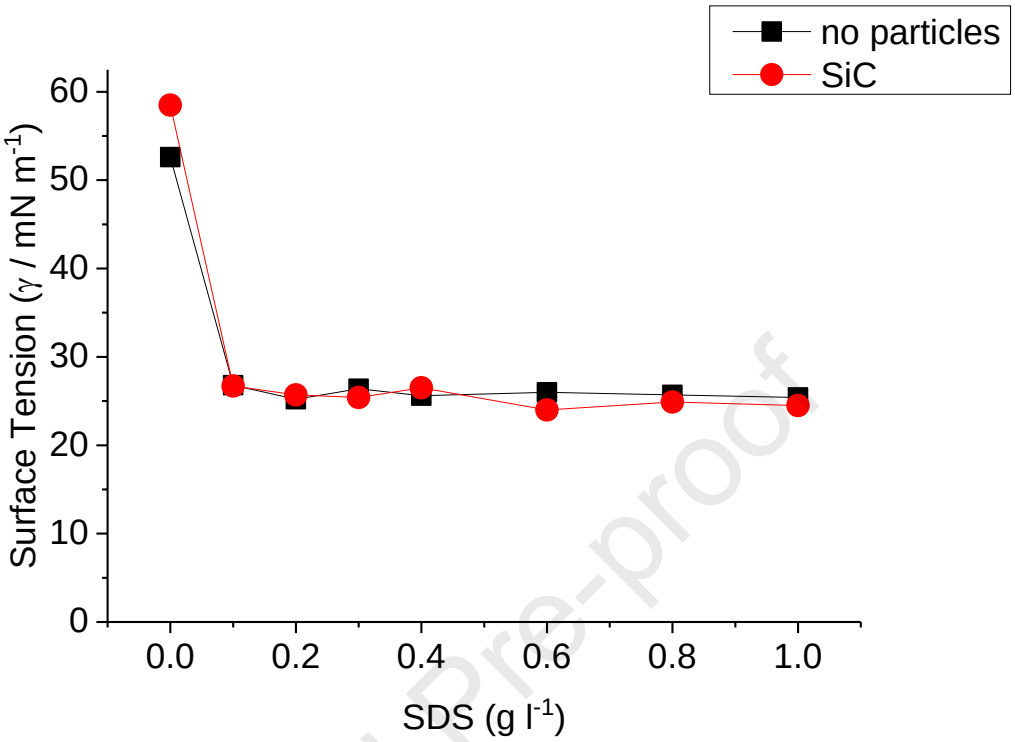

Figure 10(a-d): Schematic diagram showing a) SiC nanoparticle and ion cloud attracted from bulk by electrophoretic force, F, to anodic working electrode, WE, which exhibits a partial layer of adsorbed SDS molecules b) the SiC particle moves close to the anode and its cloud of ions interacts with the surface, c) magnification of region between SiC particle and anodic WE showing presence of H^+ and Co^{2+} ions and DS ions adsorbed on both particle and WE, d) cathodic WE reduces H^+ and Co^{2+} ions and particle becomes adsorbed and encapsulated. SDS are repelled from surface [colour print]

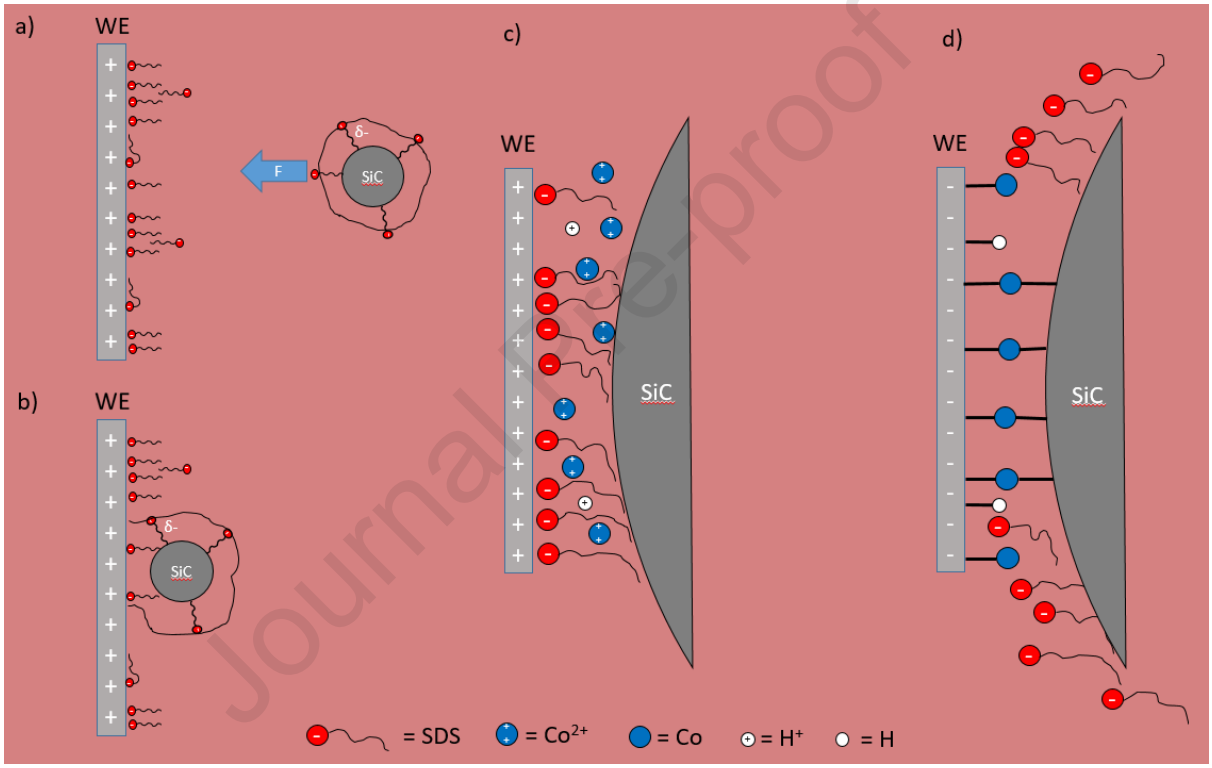

Figure 10(e): Schematic of particles attracted to anodic WE in presence of excess SDS (> 0.6 g L^{-1}) [colour print]

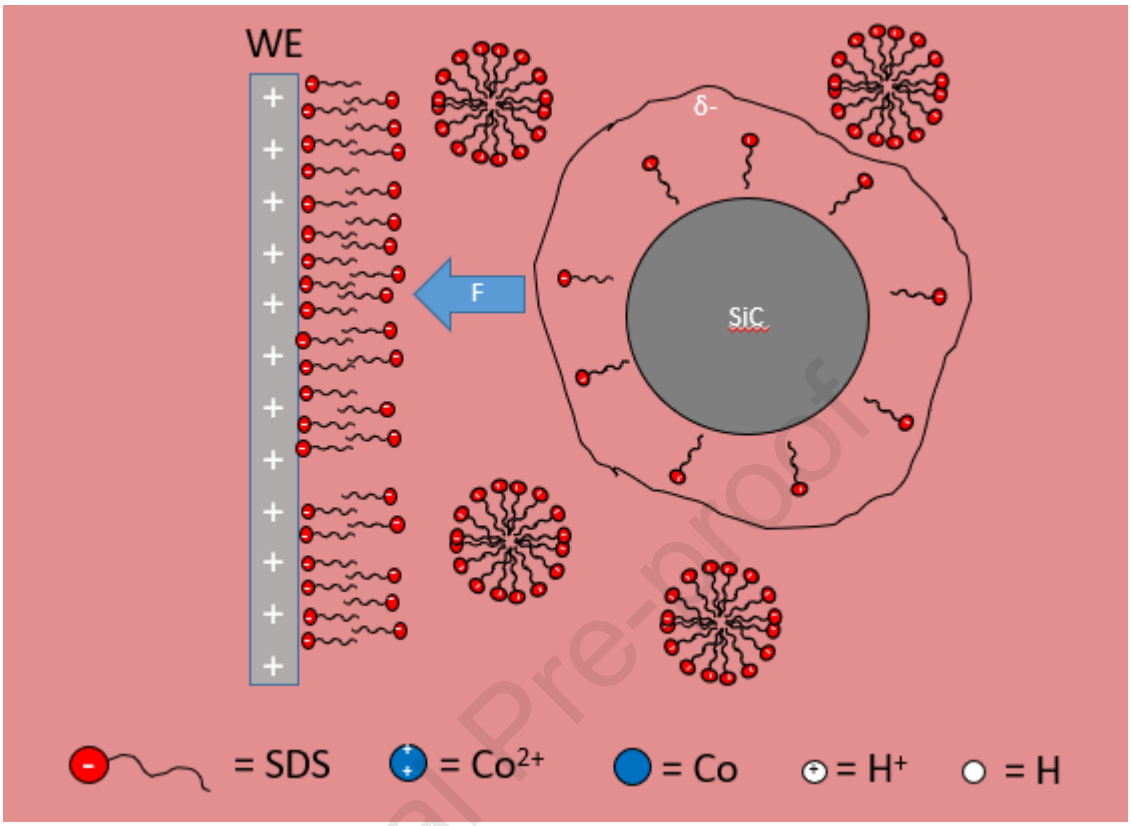

Table 2: Area of coverage by SDS

SDS / g l^{-1}	SDS / mM	Area / m^2
0.2	0.69	166
0.4	1.39	332
0.6	2.08	499
0.8	2.78	665
1.0	3.47	831

Figure 11: Plot of fractional area of coverage of working electrode surface by a) total nanoparticles plotted against the coating thickness per cycle normalised to particle diameter and b) nanoparticles present purely due to anodic pulse, plotted against the coating thickness normalised to coating diameter. [colour print]

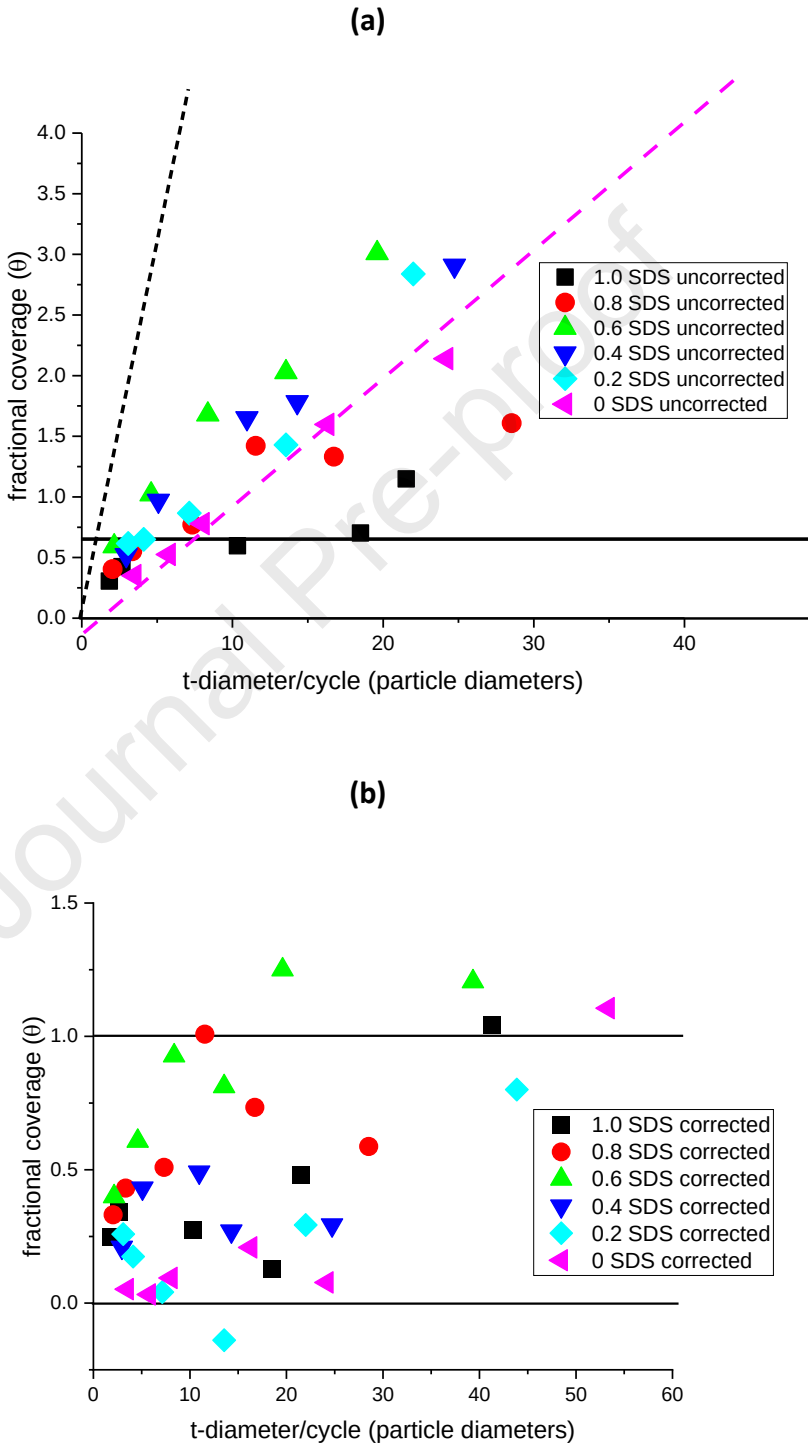

Figure 12: Graph showing the nanoparticle content of coatings against coating thickness from current Co-SiC work and previous C-WS_2 and Co-Al_2O_3 work, all produced with 0.2 g L^{-1} SDS [colour print]

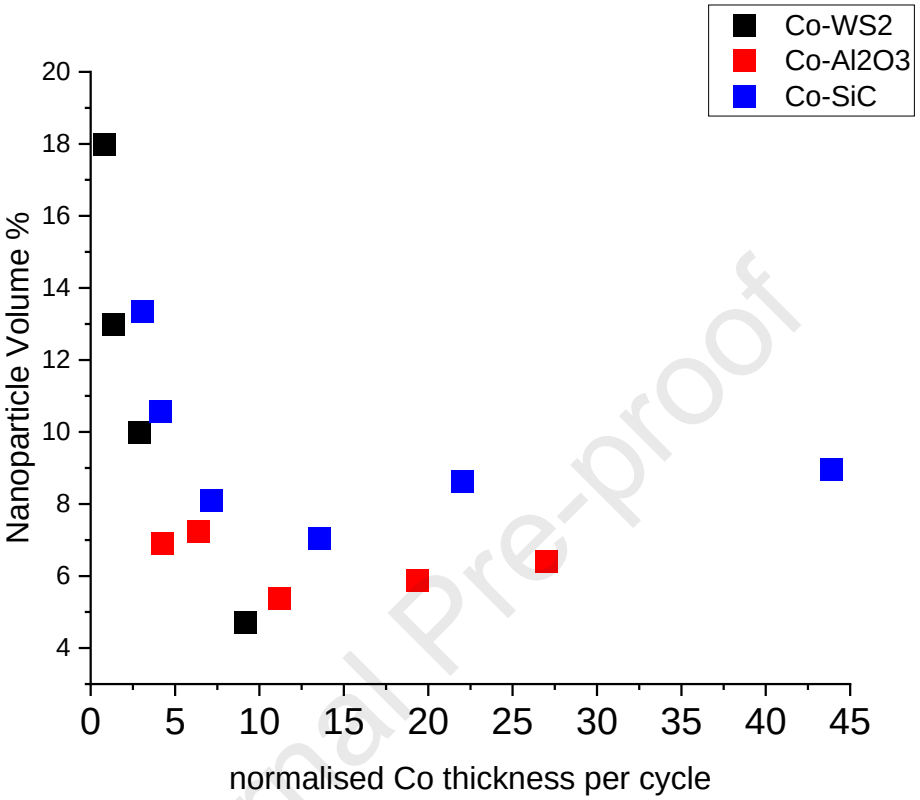

Highlights

Electrodeposited nanocomposite coatings with controllable particle content

Particle content controlled by adjusting pulse reverse plating parameters

Bath composition is designed to avoid oxide/hydroxide formation

Pulse-Reverse-Plating provides a particle delivery mechanism to working electrode

Dr. David Weston
School of Engineering
Lecturer in Materials Engineering
University Road
Leicester
LE1 7RH

6th January 2023

Dear Editor,

The authors have no competing interests to declare.

On behalf of the authors,

Yours sincerely,

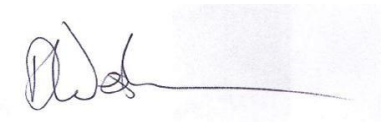

Dr. David Weston

University of Leicester, University Road, Leicester, LE1 7RH, United Kingdom
Tel: +44 (0) 116 252 2524; E-mail: dpw14@le.ac.uk